High-field properties of carbon-doped MgB_2 thin films by hybrid physical–chemical vapor deposition using different carbon sources

Supercond. Sci. Technol. **24** (2011) 125014 (12pp) doi:10.1088/0953-2048/24/12/125014

High-field properties of carbon-doped MgB_2 thin films by hybrid physical–chemical vapor deposition using different carbon sources

Wenqing Dai[1], V Ferrando[1], A V Pogrebnyakov[1], R H T Wilke[1,2], Ke Chen[1,7], Xiaojun Weng[2,3], Joan Redwing[2,3], Chung Wung Bark[4], Chang-Beom Eom[4], Y Zhu[4], P M Voyles[4], Dwight Rickel[5], J B Betts[5], C H Mielke[5], A Gurevich[6], D C Larbalestier[6], Qi Li[1] and X X Xi[1,2,3,7]

[1] Department of Physics, The Pennsylvania State University, University Park, PA 16802, USA
[2] Materials Research Institute, The Pennsylvania State University, University Park, PA 16802, USA
[3] Department of Materials Science and Engineering, The Pennsylvania State University, University Park, PA 16802, USA
[4] Department of Materials Science and Engineering, University of Wisconsin, Madison, WI 53706, USA
[5] National High Magnetic Field Laboratory, Los Alamos National Laboratory, Los Alamos, NM 87545, USA
[6] Applied Superconductivity Center, National High Magnetic Field Laboratory, Tallahassee, FL 32310, USA

Received 12 September 2011
Published 9 November 2011
Online at stacks.iop.org/SUST/24/125014

Abstract

We have studied the high-field properties of carbon-doped MgB_2 thin films prepared by hybrid physical–chemical vapor deposition (HPCVD). Carbon doping was accomplished by adding carbon-containing gas, such as bis(methylcyclopentadienyl)magnesium and trimethylboron, into the hydrogen carrier gas during the deposition. In both cases, T_c drops slowly and residual resistivity increases considerably with carbon doping. Both the a and c lattice constants increase with carbon content in the films, a behavior different from that of bulk carbon-doped MgB_2 samples. The films heavily doped with trimethylboron show very high parallel H_{c2} over 70 T at low temperatures and a large temperature derivative $-dH_{c2}^{\parallel}/dT$ near T_c. These behaviors are found to depend on the unique microstructure of the films, which consists of MgB_2 layers a few-nanometers thick separated by non-superconducting MgB_2C_2 layers. This leads to an increase in the parallel H_{c2} by the geometrical effect, which is in addition to the significant enhancement of H_{c2} due to changes in the scattering rates within and between the two bands present in films doped using both carbon sources. The high H_{c2} and high-field $J_c(H)$ values observed in this work are very promising for the application of MgB_2 in high magnetic fields.

(Some figures may appear in colour only in the online journal)

1. Introduction

Since the discovery of 39 K superconductor MgB_2 [1], much effort has been made to prepare this material for high magnetic field applications [2, 3]. The relatively low upper critical field H_{c2} (~5 T for the perpendicular field and ~20 T for the parallel field at low temperature [4]) and the rapid suppression of critical current density J_c by a magnetic field in undoped MgB_2 impair these applications [2–6]. There have been many attempts to enhance the high-field performance of MgB_2,

[7] Present address: Department of Physics, Temple University, Philadelphia, PA 19122, USA.

including using irradiation [7] and adding dopants such as carbon [8], SiC [9] and ZrB_2 [10]. Among these methods, carbon doping has proven to be an effective way to enhance H_{c2} and high-field J_c [11, 12]. In bulk samples carbon doping has been shown to enhance H_{c2} values in both $H \parallel c$ and $H \parallel ab$ directions and reduce the anisotropy ratio [13]. An even more dramatic enhancement of H_{c2} has been seen in the case of carbon-doped MgB_2 films produced by hybrid physical–chemical vapor deposition (HPCVD) [14, 15], where H_{c2} values as high as 70 T for $H \parallel ab$ and 40 T for $H \parallel c$ have been reported [16, 17]. A metalorganic (MO) precursor bis(methylcyclopentadienyl)magnesium [$(MeCp)_2Mg$] was used as the source of carbon in these reports [16, 17]. Such high H_{c2} values have not been reproduced in carbon-doped MgB_2 bulk samples and the physical mechanism behind the larger H_{c2} values in thin films is not yet well understood. A TEM study proposed that the c-axis tilt in these carbon-alloyed MgB_2 thin films disturbs $p_z\pi$ orbits of MgB_2, causing strong π band scattering, which may be the origin of the exceptional high $H_{c2}^{\parallel}(0\ \mathrm{K})$ [18]. Carbon-alloying also improves high-field critical current density $J_c(H)$ and irreversibility field H_{irr} in HPCVD films [19]. However, the doped films have highly resistive amorphous grain boundaries, which lead to reduced J_c [14, 15]. Using a hot-filament assistant (HFA) HPCVD and methane source, Zhuang *et al* fabricated carbon-doped MgB_2 films with better grain connectivity without sacrificing high H_{c2} [20]. Microstructural analysis showed that the improvement of grain connectivity in such films is due to the formation of a MgB_2C_2 layer on top of the MgB_2 layer instead of in the grain boundaries. The high H_{c2} in these HFA-HPCVD samples is attributed to the anomalous π-band scattering which may be a result of the strained MgB_2 lattice caused by thin MgO nanoplatelets [21].

According to a two-band dirty limit theory, H_{c2} of the two-gap superconductor MgB_2 depends on the relative strength of scattering within the two bands and can be enhanced well above the estimated $H_{c2}(0) = 0.69T_cH'_{c2}(T_c)$ of one-gap theory by tuning the σ and π band scattering [22]. In both the MO source and methane source doping cases, HPCVD films show much higher H_{c2} values than bulk samples with strong π-band scattering [16, 21], although TEM studies suggest that the strong π-band scatterings in the two types of films are caused by different structural disorders [18, 21]. It is of both scientific significance and technological interest to understand the underlying mechanism of the H_{c2} enhancement in carbon-doped MgB_2 films. Further, it is desirable to be able to manipulate the interband and intraband scattering in a controllable manner. In this paper, we report the result of doping MgB_2 using a new carbon source, trimethylboron [$B(CH_3)_3$, or TMB], which shows a different microstructure than in the previously reported films doped using other carbon sources. A remarkably large parallel H_{c2} slope near T_c $[-(dH_{c2}^{\parallel}/dT)_{T_c} \sim 8.3\ \mathrm{T\ K^{-1}}]$ and an increased H_{c2} anisotropy $\gamma = H_{c2}^{\parallel}/H_{c2}^{\perp}$ with doping were observed in these films. The results are compared systematically with those in films doped with the MO source. The different behaviors of H_{c2} are attributed to the unique microstructural characteristics in these films doped using different carbon sources.

2. Experimental details

Carbon-doped MgB_2 films of thickness 100–200 nm were grown on SiC (0001) substrates by the HPCVD method, which has been described in detail previously [23, 24]. For carbon doping, a carbon-containing gas was added to the gas stream as the carbon source. Results from two different carbon sources, the MO $(MeCp)_2Mg$ and TMB (2.0% balanced in hydrogen), are presented in this work. For the case of the MO source, the carbon concentration was controlled by adjusting the rate of a secondary hydrogen flow passing through the $(MeCp)_2Mg$ bubbler. The flow rate of TMB was varied from 0 to 20 standard $cm^3\ min^{-1}$ (sccm) to control the doping level in the films. Diborane gas (B_2H_6, 5.0% in hydrogen) was used as the boron source and its flow rate was 10 sccm. Hydrogen was used as the carrier gas, and its gas flow was adjusted to keep the total gas flow at 450 sccm. The pressure in the reactor chamber during the deposition was 73 Torr. All the films were deposited at about 720 °C.

All the undoped and carbon-doped MgB_2 films on (0001) SiC substrates grow with their c-axis normal to the substrate surface. We measured their in-plane and out-of-plane lattice parameters with a four-circle x-ray diffractometer (Bruker-AXS). The in-plane and out-of-plane lattice parameters were determined from the $MgB_2(10\bar{1}1)$ and (0002) diffraction peaks while the peaks from SiC substrate were used as internal standards. Several $(10\bar{1}1)$ and (0002) family peaks were used in order to minimize errors. The peak position in each diffraction profile was determined by fitting to the pseudo-Voigt function. The atomic per cent carbon contents in a series of films were determined by using wavelength dispersive x-ray spectroscopy (WDS) to establish a correlation between the carbon concentrations in the films and the $(MeCp)_2Mg$ or TMB flow rates during deposition, which was used to determine the nominal carbon concentrations in this study.

The TEM study of the films doped with $(MeCp)_2Mg$ was carried out at the University of Wisconsin. Plan-view TEM samples were prepared by mechanical polishing into a thin wedge. Polishing was performed under polishing oil instead of water to reduce damage during thinning. Plan-view TEM images were acquired on a Philips CM200 Ultratwin TEM at 200 kV with a nominal Scherzer resolution of 0.2 nm. The TEM of carbon-doped films with TMB was studied at the Pennsylvania State University. Cross-sectional TEM specimens were prepared using mechanical polishing followed by argon ion milling. Cross-sectional TEM and electron diffraction were carried out on a JEOL 2010F field-emission TEM operated at 200 kV.

For the films doped with TMB, photolithography and Ar ion-beam milling were used to pattern the samples into 200 μm long, 10 μm wide and about 100 nm thick bridges for transport measurement. A MgO layer of about 10 nm was sputtered on top of the bridges to prevent sample degradation by moisture. The samples were first measured in a Quantum Design Physical Properties Measurement System (PPMS) with a 9 T superconducting magnet. Unless noted otherwise, the upper critical field H_{c2} was extracted from resistivity versus temperature curves under different fields using the 90%

of normal residual resistivity criterion. The critical current density J_c was determined by transport measurement, defined by a DC voltage criterion of 1 μV (corresponding to an electric field criterion of 50 μV cm^{-1}). For the dependence of J_c on angle θ between the c-axis of the films and magnetic field B, the current and the magnetic field were kept perpendicular to each other. High-field H_{c2} was obtained by measuring resistance versus field sweeps at various temperatures at the National High Magnetic Field Laboratory (NHMFL) at Florida State University (up to 33 T) and Los Alamos National Laboratory (up to 60 T).

3. Results and discussions

3.1. Transport and structural properties

The transport and structural properties of carbon-doped MgB_2 films with the MO source have been studied in detail previously [14, 15, 18]. For MgB_2 films doped with the TMB source, the resistivity versus temperature curves with different doping levels are shown in figure 1(a). Carbon doping using TMB causes a considerable increase in the resistivity while the T_c only drops slowly. The change in T_c and residual resistivity with doping level is shown in figure 1(b). The rapid increase of the residual resistivity and the slow suppression of T_c with carbon concentration resemble the previous result for carbon-alloyed MgB_2 films using a MO source by HPCVD [14, 15]. The carbon doped into the MgB_2 lattice reduces T_c. The reduction in T_c with doping can be used to estimate the amount of carbon doped into MgB_2. Based on the results for carbon-doped single crystals, a T_c of 33.5 K corresponds to a carbon concentration of ~6% in $Mg(B_{1-x}C_x)_2$ [25]. This is substantially smaller than the nominal carbon concentration for the TMB-doped film with T_c of 33.5 K, which is 33.5%. The rest of the carbon forms resistive foreign phase in the grain boundaries.

The foreign phase in the grain boundaries, most likely MgB_2C_2 [21, 26], is highly resistive and will block the current transport and reduce the connectivity between the MgB_2 grains. It will cause an increase in the experimentally measured resistivity and critical current density [27]. The MgB_2 grain connectivity can be estimated from the temperature-dependent part of the resistivity using Rowell's model [28]. The model states that the resistivity of MgB_2 samples can be fitted using the equation

$$\rho(T) = F[\Delta\rho_{sc}(T) + \rho_0] \quad (1)$$

where $\Delta\rho_{sc}(T)$ is the temperature-dependent part of the resistivity of MgB_2 single crystal, ρ_0 is the residual resistivity, and $1/F$ is the current-carrying fraction of the sample cross-sectional area indicating how well the grains are connected. Assuming that $\Delta\rho_{sc}(T)$ does not change when defects, impurities, and foreign phases are introduced into the pure MgB_2 sample, the experimentally measured $\Delta\rho \equiv \rho(300\,\mathrm{K}) - \rho(42\,\mathrm{K}) = F[\Delta\rho_{sc}] = F[\rho_{sc}(300\,\mathrm{K}) - \rho_{sc}(42\,\mathrm{K})]$ can be used to estimate the value of F. Using $\Delta\rho_{sc} = 8\ \mu\Omega$ cm, the fraction $1/F$ estimated in this way for the carbon-doped MgB_2 films by the TMB source is plotted together with the previous result for the MO source [15] in figure 2(a). Carbon

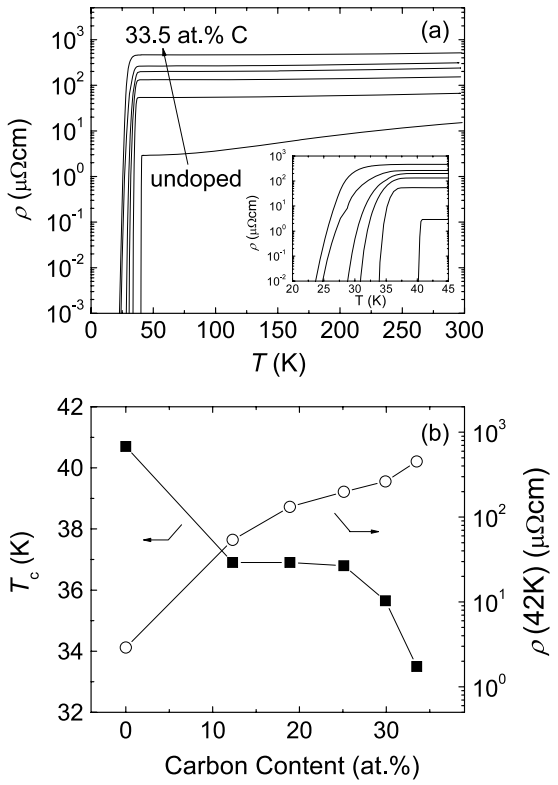

Figure 1. (a) Resistivity versus temperature curves for carbon-doped MgB_2 films using the TMB source with nominal carbon concentrations of 0, 12.3, 18.9, 25.1, 29.9 and 33.5 at.% from bottom to top. The inset shows details at the superconducting transition. (b) Superconducting transition temperature T_c and residual resistivity ρ (42 K) as a function of carbon concentration for films in plot (a).

doping reduces the fractional area of the samples. At the nominal carbon concentration of 33.5%, $1/F$ is ~0.16—a reduction of the connectivity to about 1/6 of its original value. The dependence of the current-carrying fractional area of the carbon-doped films by TMB is comparable to that of the previous films doped by the MO source, in particular for high carbon concentrations. However, this is far from sufficient to explain the rapid increase in sample resistivity. For example, while the current-carrying fractional area reduces by only about a factor of 6 in a film with 33.5% nominal carbon content, the sample residual resistivity increases by over two orders of magnitude.

A more accurate way to estimate the grain connectivity is to use the reduction of self-field J_c as carbon is doped into the MgB_2 films. According to Rowell *et al*, J_c in MgB_2 samples with reduced grain connectivity is limited by the same area factor as the resistivity [27]. Assuming that the self-field J_c does not change with doping, a decrease in the connectivity will reduce the experimentally measured J_c by a factor of F:

$$J_c = J_{c0}/F \quad (2)$$

where J_{c0} is the self-field critical current density of the perfectly connected samples. Figure 2(b) shows $1/F$ versus the carbon content estimated using the J_c data shown in figure 14. For the nominal carbon concentration of 29.9%,

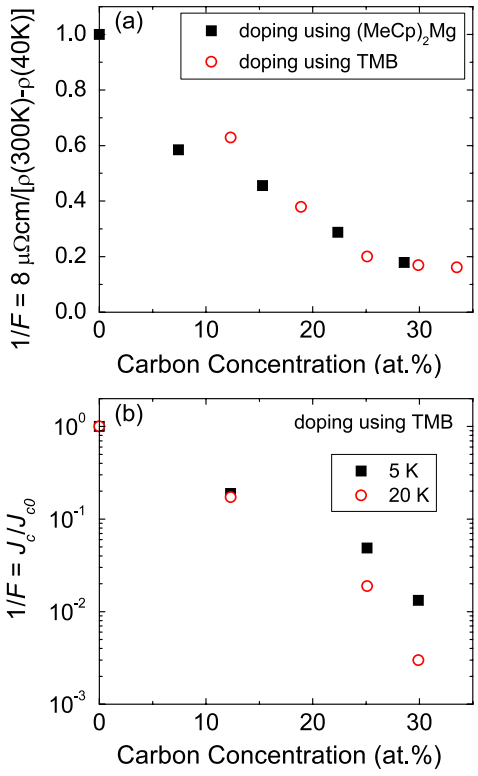

Figure 2. (a) MgB_2 fractional area estimated using equation (1) versus carbon concentration for films doped by a $(MeCp)_2Mg$ source [15] and TMB source. (b) MgB_2 fractional area extracted from the self-field J_c at 5 and 20 K as a function of carbon concentration for MgB_2 films doped with a TMB source.

$1/F$ is 0.013 using the self-field J_c data for $T = 5$ K, which is in a much better agreement with the experimentally measured resistivity increase in figure 1(b). However, when the 20 K self-field J_c data are used, the $1/F$ value is even smaller, overestimating the reduction in the grain connectivity. Further, the connectivity ought not to be strongly temperature dependent.

From the above analysis, we can conclude that the assumptions used in both approaches are not completely valid in dealing with the carbon doping results in our films. To correctly account for the resistivity increase, we need to assume that the phonon contribution to the resistivity (the temperature-dependent part of the resistivity) is enhanced as the result of carbon doping or that the self-field J_c of the $Mg(B_{1-x}C_x)_2$ grains is suppressed by carbon doping, in particular for higher temperatures. Despite the uncertainties about the extent of the reduction in the grain connectivity due to carbon doping, it is clear that it contributes to the enhancement of resistivity in the carbon-doped films.

TEM studies confirm the presence of a foreign phase in carbon-doped films. Figure 3 shows the results for two films doped with the TMB source. Figures 3(a) and (b) are from a lightly doped film with a nominal carbon concentration of 12.3 at.% and figures 3(c) and (d) are from a heavily doped film with a nominal carbon of 33.5 at.%. The low-magnification images show that both films have columnar grain structures, but the heavily doped film (figure 3(c)) is much more disordered than the lightly doped film (figure 3(a)). In addition, stripes parallel to the film surface are seen in the heavily doped film, but are absent in the lightly doped film, as well as in films doped with the MO source [18]. The selected area diffraction (SAD) images collected from both films show diffraction spots from the MgB_2 as well as the MgB_2C_2 phases. The intensity of the diffraction spots corresponding to MgB_2C_2 is stronger in the 33.5% nominal carbon sample (figure 3(d)) than in the less doped sample (figure 3(b)), indicating a higher volume percentage of the MgB_2C_2 phase in the heavily doped sample. The existence of the MgB_2C_2 foreign phase in the carbon-doped MgB_2 films is consistent with previously reported carbon-doped MgB_2 samples [21, 29] and also agrees with the theoretical calculations [26]. The vertical streaks in figure 3(d) are caused by the small stripes as shown in figure 3(c). The radial arcs in the SAD patterns of both samples are similar to what was observed in the MO-doped films [18]. They indicate distribution in the local c-axis of the film away from the substrate normal. In addition, both $MgB_2[1\bar{1}00]$ and $[11\bar{2}0]$ spots are visible in the diffraction pattern, which suggests that some of the MgB_2 grains rotate 30° about the c-axis. This has been reported in the films doped with the MO source [18] and is shown in the plan-view TEM images in figure 4. Near the top surface, the MO-doped films show a microstructure of columnar nanograins that are separated by amorphous regions. Cross-sectional images [18] show better connectivity of the nanograins near the substrate. Figure 4(b) shows that some of the grains are rotated by 30° about [0001] with respect to others, and with respect to the substrate. Electron energy-loss spectroscopy (EELS) measurement shows that the carbon content in the $Mg(B_{1-x}C_x)_2$ grains is $\leqslant$5%, and most of the carbon in the film is in the C-rich amorphous second phase in the grain boundary [18]. No stripes like those in figure 3(c) are observed.

The lattice constants of films carbon-doped by TMB and the MO source (from [14]) as a function of nominal carbon concentration are plotted in figure 5. In both cases, the out-of-plane lattice constant c expands with increasing carbon content and the values are similar, except that in films heavily doped by TMB a jump occurs around 20 at.% and the c lattice constant becomes larger than for the MO films. For the in-plane lattice constant a, we were able to measure only one TMB film with a nominal carbon concentration of 12.3 at.% due to the poor crystalline quality of more heavily doped samples. Still, the a lattice constant displays a trend of increase with carbon doping as in the carbon-alloyed films doped by the MO source. Carbon doping of HPCVD films by both sources causes expansions in both the c and a lattice constants, different from the carbon-doped MgB_2 bulk samples and single crystals where the a lattice constant decreases and the c lattice constant remains unchanged with carbon doping [30]. Saengdeejing *et al* proposed that the behavior of the lattice parameters in MgB_2 thin films upon carbon doping is the result of the difference in the coefficient of thermal expansion between $Mg(B_{1-x}C_x)_2$ and the amorphous MgB_2C_2 phase in the grain boundaries [26]. Bengtson *et al* also suggested that the carbon incorporated in the MgB_2 lattice cannot explain the change of lattice parameters in thin films and unincorporated carbon or other factors lead to the effect [31].

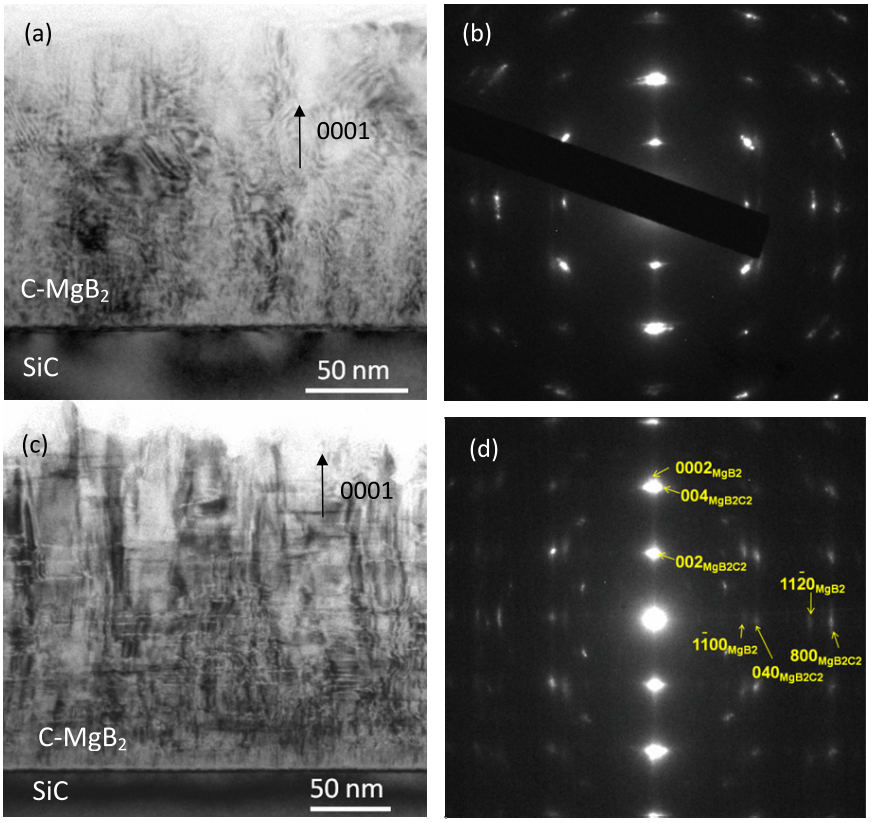

Figure 3. TEM images of MgB_2 films carbon-doped by TMB taken along the SiC [1$\bar{1}$00] zone-axis: low-magnification cross section (a) and SAD pattern (b) taken from of a low doping film with nominal carbon concentration of 12.3 at.%. Low-magnification cross section (c) and SAD pattern (d) of a heavily doped film with nominal carbon concentration of 33.5 at.%.

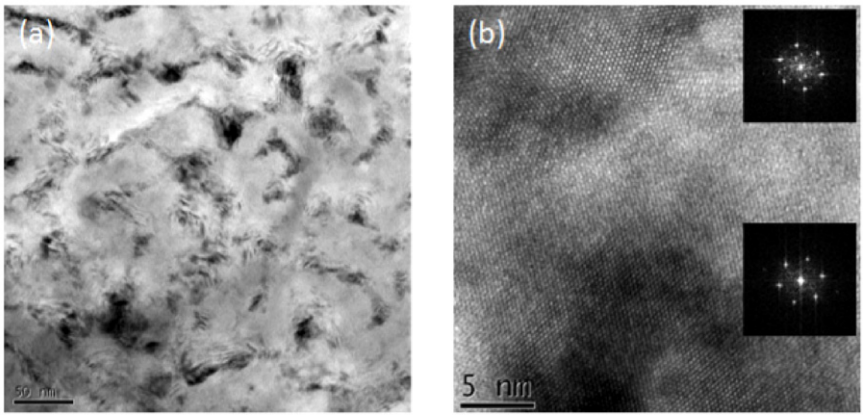

Figure 4. TEM images of the MgB_2 films carbon-doped using $(MeCp)_2Mg$ source. (a) A plan-view image along the [0001] direction of the top surface of the film. The dark grains are crystalline MgB_2, and gray material in between is amorphous. (b) HRTEM image along [0001] showing two crystal grains and the intervening amorphous material. The inset diffractograms of the two grains show a 30° rotation about [0001]. The corresponding diffraction patterns are given in [18].

3.2. Upper critical field of films doped with the MO source

The $H_{c2}(T)$ of the MO-doped films up to 9 T has been previously reported [14]. Here, we report the result of H_{c2} measurements in high magnetic field up to 60 T. In figure 6, H_{c2} of four MO films is shown as a function of temperature for both parallel (open symbols) and perpendicular (solid symbols) fields. The nominal carbon concentrations are (a) 6, (b) 23, (c) 24 and (d) 33 at.%. The criterion used for the determination of H_{c2} for this figure is the onset of the superconducting transition as it is the most appropriate for comparing with theory, in which H_{c2} is a thermodynamic parameter. However, because of the extraordinarily high H_{c2} we were not able to obtain the low temperature data for some samples. The solid lines in the figure are fits using the dirty two-band theory [22], which predicts that the temperature

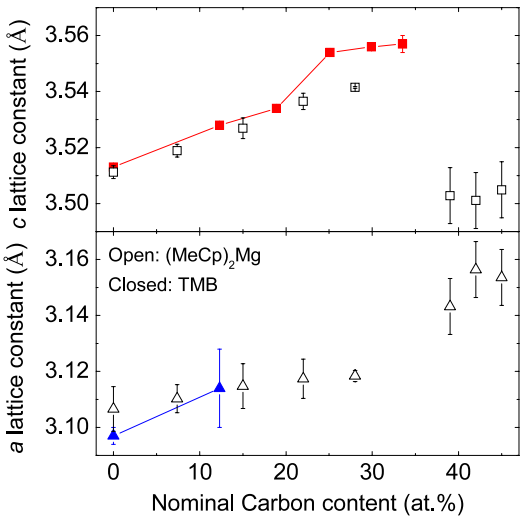

Figure 5. The c-axis lattice constant and a-axis lattice constant of the MgB_2 films carbon-doped by a TMB source (closed) (a-axis lattice constant data from [31]) and a $(MeCp)_2Mg$ source (open) [14] as a function of nominal carbon content. The lines are guides to the eye.

dependence of the upper critical field depends on the relative strengths of the two intraband electron diffusivities D_σ and D_π in the σ and π bands, respectively. Whereas near T_c the temperature dependence of H_{c2} depends on the greater of the two diffusivities, in the low temperature limit H_{c2} is determined by the band with the smaller diffusivity. Thus an important quantity that influences the temperature dependence of H_{c2} is $q \equiv D_\pi/D_\sigma$. In figure 6, the q values for both the parallel and perpendicular field, $q^{\parallel}$ and $q^{\perp}$, respectively, as well as the interband scattering parameter $g = \Gamma/4\pi T_{c0}$, where Γ is the interband scattering rate, all obtained from the fit to the two-band theory, are given for each sample. The four films show different behaviors. Whereas films 1 and 3 have q values less than one, indicating that the diffusivities in the σ band are greater than in the π band, films 2 and 4 have q values greater than one, indicating greater diffusivities in the π band. That is, of the four MO films, two have dirtier π bands and two have dirtier σ bands. No systematic change of relative diffusivity with doping level was observed in these four samples. While film 1 shows an upturn in perpendicular H_{c2} at low temperature, other samples do not show such a tendency. Film 3 has high H_{c2} values for both the parallel and perpendicular fields, whereas the perpendicular field values for the other films are much lower.

Both interband and intraband scattering can be changed by carbon doping, and they are very sensitive to the detailed microstructures of the samples [32–34]. As pointed out by Eisterer in a review of a large body of data from the literature [3], defects and impurities reduce the mean free path in both bands and sample to sample variations are large. The large scatter of data from the literature was attributed to the details of the defect structures in different samples. In the present case of carbon-doped MgB_2 films, the amount of carbon doped into the $Mg(B_{1-x}C_x)_2$ grains and the introduction of foreign phases in the grain boundaries can

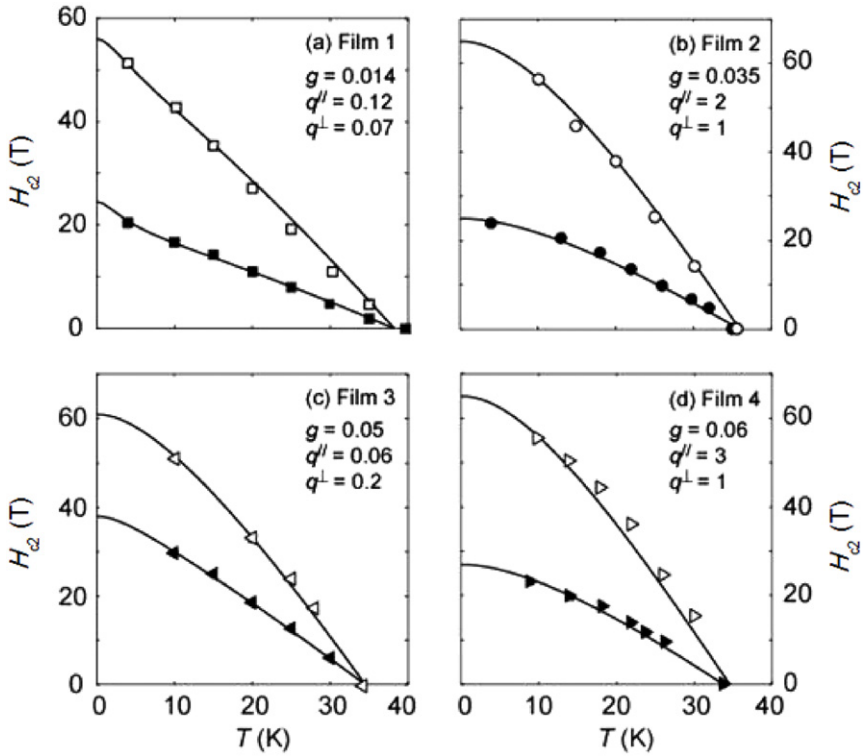

Figure 6. Temperature dependence of the upper critical field H_{c2} of four different carbon-doped MgB_2 films using a $(MeCp)_2Mg$ source with nominal carbon concentrations of 6, 23, 24 and 33 at.% from (a) to (d). Open dots are for a parallel field and closed dots for a perpendicular field direction. The lines are fits using two-band dirty limit theory. g is the interband scattering parameter. q is the relative diffusivity rate for the π band to the σ band.

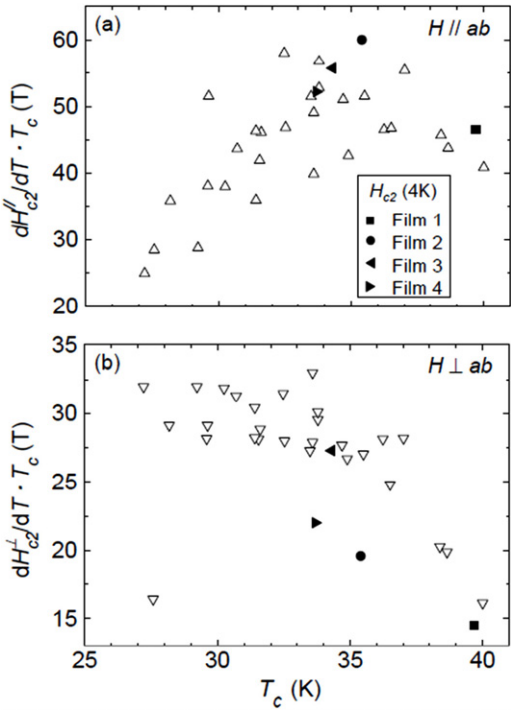

Figure 7. The product $dH_{c2}/dT \cdot T_c$ versus T_c for clean and carbon-alloyed MgB_2 films using $(MeCp)_2Mg$ source. The criterion for H_{c2} is $\rho(H_{c2}) = 0.9\rho_0$. The slope $dH_{c2}/dT \cdot T_c$ is taken from data between 1 and 9 T. Data points for the four films marked by solid symbols are from actual measurements of H_{c2} (4 K).

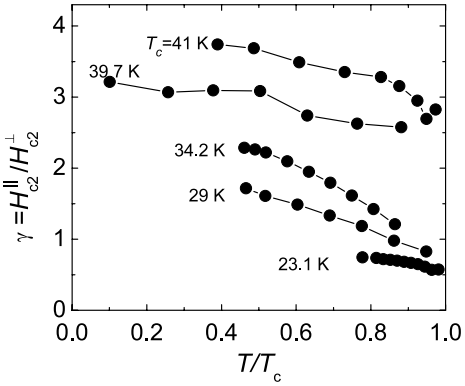

Figure 8. H_{c2} anisotropy γ as a function of normalized temperature for carbon-doped MgB_2 films using $(MeCp)_2Mg$ source.

all be influenced by the details of the deposition conditions. These impurity and defect structures, as well as the strain due to the difference in the coefficient of thermal expansion between $Mg(B_{1-x}C_x)_2$ and the amorphous MgB_2C_2 phase in the grain boundaries, will affect the intraband and interband scattering and their relative significance in each sample leads to its distinct behavior. To gain a better control of these parameters through optimized processing conditions is the goal of further studies. For example, for high H_{c2} in both parallel and perpendicular fields, one would tune the interband and intraband scattering similar to those in film 3, i.e. a dirtier π band and relatively high interband scattering.

Given the lack of a complete control of the sample properties in our deposition process, we rely on the large collection of data from many samples to study statistically the H_{c2} behavior of MgB_2 films carbon-doped with the MO source. In figure 7 we plot the dependence of $dH_{c2}/dT \cdot T_c$, in both parallel (figure 7(a)) and perpendicular fields (figure 7(b)), on T_c of the sample for a large number of films doped by the MO source. In general, a lower T_c corresponds to a higher carbon content in the sample. This data set includes samples that were measured only in fields up to 9 T, for which the function $dH_{c2}/dT \cdot T_c$ was used to gain a rough estimate of $H_{c2}(T = 0)$. In fact, depending on the relative diffusivity, the shape of the $H_{c2}(T)$ curve can be very different from the Bardeen–Cooper–Schrieffer (BCS) behavior in single-gap superconductors, thus $dH_{c2}(0)$ is very different from $dH_{c2}/dT \cdot T_c$. The scatter in the figure reflects the wide range of difference in the relative strength of intraband scattering rates among the samples as illustrated in figure 6. Even with the scatter of data, trends in T_c dependence can be seen. For the parallel field a peak of about 60 T appears around the T_c of 35 K, whereas for the perpendicular field $dH_{c2}/dT \cdot T_c$ increases with carbon content and saturates at about 30 T. Similar T_c dependence of H_{c2} with a peak at about 35 K has been found in a report of MgB_2 samples disordered by radiation [35]. When expressed as a function of reduced T_c, T_c/T_{c0}, the same dependence is found even in irradiated A15 superconductors. This shows that, in general, H_{c2} increases with increasing disorder until the suppression of superconducting condensation energy prevails, causing T_c and thus H_{c2} to go down [35].

In addition to influencing the temperature dependence of H_{c2}, the changes in the relative scattering rates are predicted to change the temperature dependence of the anisotropy ratio $\gamma = H_{c2}^{\parallel}/H_{c2}^{\perp}$. Pure MgB_2 exhibits a moderately high anisotropy near 6 at low temperatures, monotonically decreasing with temperature to near 2 at T_c [36]. In the dirty limit, a monotonic decrease in the anisotropy ratio with increasing temperature is predicted for $D_\pi \gg D_\sigma$ and the reverse, i.e. a monotonically increasing γ with increasing temperature, for $D_\pi \ll D_\sigma$ [22]. Figure 8 shows the temperature dependence of γ for several films with different carbon contents and T_c values. All films show a decrease in γ with increasingly reduced temperature T/T_c. The γ value decreases with decreasing T_c, thus increasing carbon content; however, there is no definitive change in the temperature dependence of γ. The result suggests that an increase in the intraband scattering, whether in the π-band or the σ-band, decreases the anisotropy of the upper critical field, consistent with polycrystalline and single crystal samples [3].

3.3. High-field properties of films doped with TMB

The high-field behaviors of MgB_2 films doped with TMB are very different from those of MO-doped films in many aspects. Figure 9(a) shows the temperature dependence of H_{c2} near T_c measured in a 9 T magnet for an undoped film and two samples with different carbon contents doped using TMB. As the carbon content increases, the slope of $H_{c2}(T)$ becomes steeper for both perpendicular and parallel fields. Figures 9(b) and (c) plot the parallel and perpendicular $H_{c2}(T)$ slope near

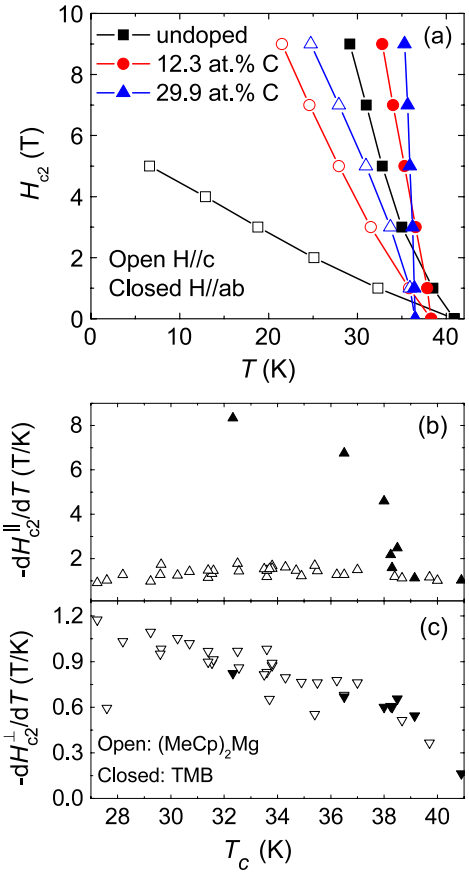

Figure 9. (a) Upper critical field H_{c2} near T_c as function of temperature T for undoped film and two films doped using a TMB source with nominal carbon concentration of 12.3 and 29.9 at.%. (b), (c) Temperature derivative of parallel and perpendicular H_{c2} near T_c as a function of T_c for carbon-doped MgB_2 films using a $(MeCp)_2Mg$ source (open triangles) and a TMB source (closed triangles).

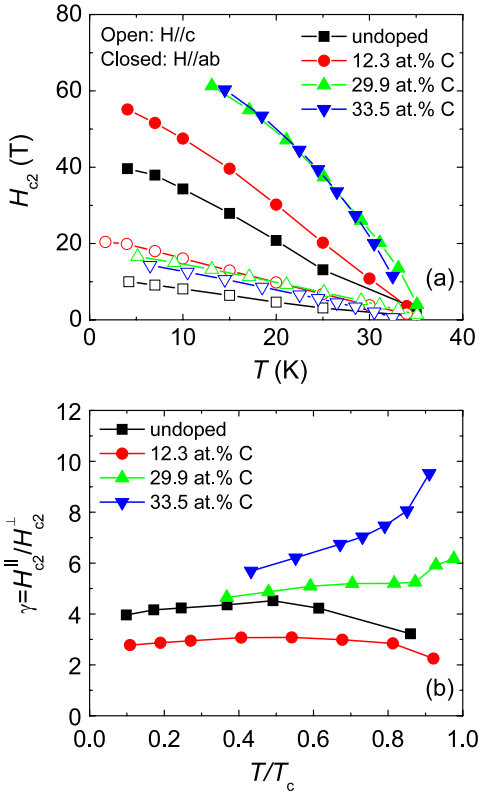

Figure 10. (a) Upper critical field H_{c2} versus temperature T curves of undoped film and three films doped using a TMB source measured in pulsed field facility in LANL. The nominal carbon concentrations are 0, 12.3, 29.9 and 33.5 at.%, respectively. (b) Normalized temperature dependence of H_{c2} anisotropy γ for the four films in plot (a). The lines are guides to the eye.

T_c as a function of T_c for carbon-doped MgB_2 films using TMB (closed dots) together with the result for films doped with the MO source (open dots). While the perpendicular field results for both doping sources are very similar (see figure 9(c)), the parallel $H_{c2}(T)$ slope is much higher for films doped using TMB when T_c is lower than ~38 K (see figure 9(b)). A remarkable $-dH_{c2}^{\parallel}/dT$ value of 8.3 T K^{-1} was obtained for a heavily doped film with T_c at 32.3 K, substantially higher than any previously reported carbon-doped MgB_2 samples [11, 16, 20]. The largest temperature derivative of H_{c2} in a perpendicular direction near T_c by TMB doping is about 0.8 T K^{-1} for a film with nominal carbon content of 33.5 at.%.

Figure 10(a) shows the result of H_{c2} measured up to 60 T in a pulsed field at the NHMFL at Los Alamos National Laboratory (LANL) for four different films doped by TMB. The enhancement of the parallel H_{c2} by carbon doping saturates at about 30 at.%, whereas the highest perpendicular H_{c2} occurs in the sample with 12.3 at.% carbon. The $H_{c2}^{\parallel}$ values for the two heavily doped samples—nominal carbon concentrations of 29.9 and 33.5 at.%—are already close to 60 T at 15 K, approaching the BCS paramagnetic limit H_p^{BCS} [T] = $1.84T_c$ [K] [37]. It is worth noting here that the measured H_{c2} values are much lower than the estimation from the H_{c2} slope near T_c using the formula $H_{c2}(0) = 0.69T_cH'_{c2}(T_c)$. For films heavily doped by TMB, the parallel $H_{c2}(T)$ curve exhibits a downward curvature following the high H_{c2} slope near T_c, which differs from the Ginzburg–Landau (GL) linear temperature dependence [22]. For the perpendicular $H_{c2}^{\perp}$, the maximum value at 12.3 at.% carbon is about 20 T at low temperatures.

The H_{c2} anisotropy $\gamma = H_{c2}^{\parallel}/H_{c2}^{\perp}$ as a function of the reduced temperature is plotted in figure 10(b) for the four films. As the carbon content increases, γ first decreases, but then rises to larger values for heavily doped films. The increasing anisotropy of H_{c2} with carbon doping contradicts previous reports, including those of HPCVD films doped by the MO source, where carbon doping always causes γ to decrease [3, 13, 16, 38]. The temperature dependence of γ for heavily doped films is also different from the undoped and low doping films.

The high-field properties of the films heavily doped by TMB are unusual. The parallel H_{c2} at low temperature is very high, close to the BCS paramagnetic limit, and its temperature derivative near T_c is very large, up to 8.3 T K^{-1}. Both are even higher than the HPCVD films doped by the MO source. Further, the anisotropy γ is larger in heavily doped samples, which cannot be explained by any existing model.

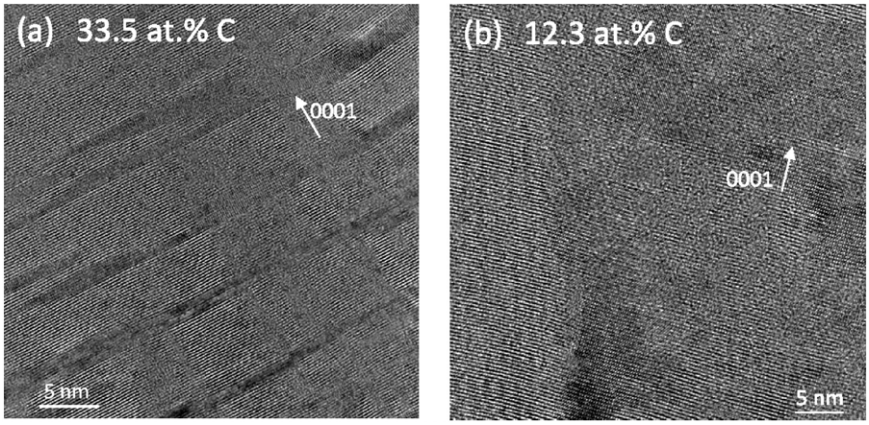

Figure 11. Cross-section HRTEM image of two films doped by TMB with nominal carbon concentrations of 33.5% (a) and 12.3% (b). Image collected along the SiC [1$\bar{1}$00] zone-axis from the same samples as in figure 3. The dark regions are the MgB_2 phase and the bright regions are the MgB_2C_2 phase.

Table 1. List of the properties of different samples. T_c, ρ and the H_{c2} slope near T_c were obtained from measurements with a Quantum Design PPMS system with a 9 T superconducting magnet. g, $q^{\perp}$ and $q^{\parallel}$ were from fitting $H_{c2}(T)$ data using two-gap dirty limit theory. g is the interband scattering parameter, $q^{\perp} = D_{\pi}^{(ab)}/D_{\sigma}^{(ab)}$, $q^{\parallel} = [D_{\pi}^{(ab)}D_{\pi}^{(c)}]^{1/2}/[D_{\sigma}^{(ab)}D_{\sigma}^{(c)}]^{1/2}$ represents the electron diffusivity ratio of the π band to σ band. D is the intraband diffusivity.

Samples	Nominal C (%)	T_c (K)	ρ (300 K) ($\mu\Omega$ cm)	ρ (40 K) ($\mu\Omega$ cm)	$(\frac{dH_{c2}^{\perp}}{dT})_{T_c}$ (T K^{-1})	$(\frac{dH_{c2}^{\parallel}}{dT})_{T_c}$ (T K^{-1})	g	$q^{\perp}$	$q^{\parallel}$
TMB4	12.3	36.9	67	54	0.59	1.8	0.03	0.093	0.122
TMB8	18.9	36.9	153	132	0.61	2.6	0.03	0.103	0.68
TMB12	25.1	36.8	238	198	0.55	4.0	0.03	0.16	0.83
TMB16	29.9	35.65	310	263	0.57	5.4	0.05	0.707	73.7[a]
TMB20	33.5	33.5	503	453	0.60	7.4	0.09	2.58	14.47[a]

[a] Fitting using an ultrathin film model with thickness 1 nm.

By a structural analysis using cross-sectional high resolution TEM (HRTEM), we found that a unique microstructure in which carbon-doped MgB_2 layers several nanometers thick are separated by non-superconducting layers exists in MgB_2 films heavily doped by TMB. Figure 11(a) shows a HRTEM image of a heavily doped film with 33.5 at.% carbon. The dark regions in the HRTEM image are identified to be the MgB_2 phase while the bright areas are the foreign phase MgB_2C_2. Long and thin MgB_2 stripes are separated in the c direction by the non-superconducting MgB_2C_2 layers. The thickness of the MgB_2 layers, though non-uniform, is around several nanometers, comparable to the estimated coherence length ξ_c. Such a multilayer structure is not seen in low doping films as shown in figure 11(b), nor in films doped with the MO source. Given this microstructural difference, it is surprising to find that the grain connectivity of the films heavily doped by TMB are basically the same as that in MO-doped films as shown in figure 2(a).

In table 1, sample properties and fitting parameters using the two-gap dirty limit theory [22] are listed for TMB-doped films with different carbon contents. Most of the experimental $H_{c2}(T)$ data can be fitted well to the theory except for $H_{c2}^{\parallel}(T)$ of the two heavily doped films. As shown in figure 12(a), the fitting curve of the parallel $H_{c2}(T)$ for the film with 33.5 at.% carbon does not reflect the large H_{c2} slope and the downward curvature near T_c. We then introduce a multilayer structure in which ultrathin MgB_2 layers are separated by insulating layers. Because the MgB_2 layers have a thickness d less than either ξ_{π} or ξ_{σ}, H_{c2} in the parallel field can be significantly enhanced and the temperature dependence of H_{c2} near T_c will be a square-root function rather than the GL linear dependence as in the bulk [22]. The sharp rise of the parallel $H_{c2}(T)$ slope in figure 9(b) when the T_c of the sample is $\sim$38 K, which may be an indication that such a multilayer structure is starting to develop. By using equations $H_{c2}^{\perp} = \frac{\phi_0}{2\pi\xi_{ab}^2(T)}$ and $H_{c2}^{\parallel} = \frac{\phi_0}{2\pi\xi_c(T)\xi_{ab}(T)}$, we estimate the coherence length ξ_c to be about 1 nm for the heavily doped films. Assuming 1 nm thick MgB_2 layers in a multilayer structure, we obtained good fitting for the parallel $H_{c2}(T)$ of the heavily doped films as shown in figure 12(b). The fitting curve extrapolates to a very high $H_{c2}^{\parallel}$ (0 K) over 70 T. However, the parameter q obtained from the fitting is very large, implying an extremely clean π band or an extremely dirty σ band. The cause and the physical meaning of the large q is not understood.

The angular dependence of critical current density $J_c(H)$ at 5 K was measured in an undoped film and a film doped with 33.5 at.% carbon and the results are plotted in figure 13. The angle θ of 90° in figures 13(a) and (c) corresponds to the parallel field direction, and $H\cos\theta$ in figures 13(b) and (d) represents the perpendicular component of the applied field. For the heavily doped film three sets of J_c data at different fields overlap on each other as shown in figure 13(b), similar to the 2D scaling behavior

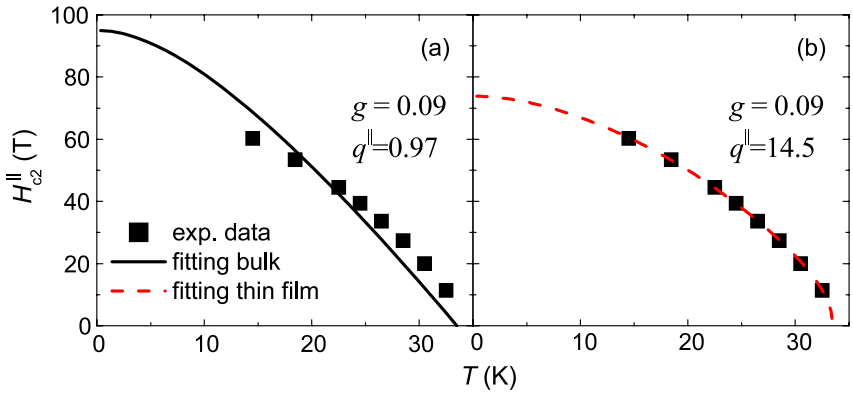

Figure 12. Theoretical fitting on temperature dependence of the parallel upper critical field H_{c2} of a film heavily doped by TMB with a nominal carbon concentration of 33.5 at.%. Solid square dots are from experimental measurements. Lines are a fitting curve from two-gap dirty limit theory using (a) a bulk model (solid line) and (b) a thin film model assuming a thickness of 1 nm (dash line). g is the interband scattering parameter. q is the relative diffusivity rate of π band to σ band.

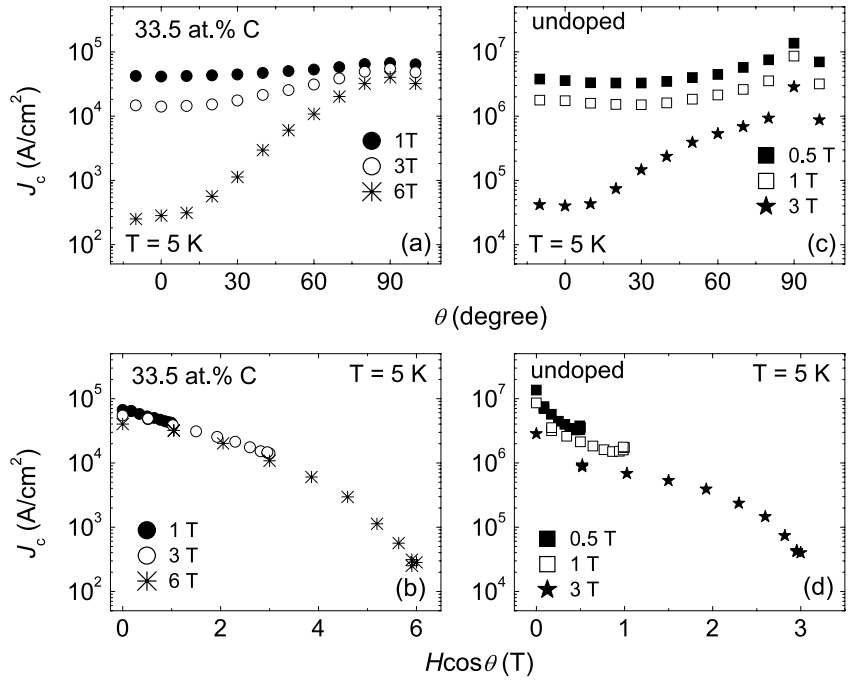

Figure 13. Angular dependence of transport critical current density under various fields $J_c(H)$ at 5 K of one film heavily doped using a TMB source with nominal carbon concentration of 33.5% (a) and one undoped film (b). Here $\theta = 0°$ corresponds to $H \parallel c$ J_c as a function of the perpendicular magnetic field component is plotted for the doped film (c) and the undoped film (d).

demonstrated in some cuprate superconductors with decoupled superconducting layers [39–42]. The undoped MgB_2 film does not show such scaling behavior (figure 13(d)). This provides further support for the layered microstructure in films heavily doped by TMB.

The transport J_c of an undoped film and three TMB-doped films with different carbon contents are plotted as a function of magnetic field H and temperature in figure 14. Similar to the case of films doped by the MO source [19], the self-field J_c of films carbon-doped by TMB decreases with increasing carbon doping level. As described earlier, the decrease can be attributed mainly to the reduction in the grain connectivity which reduces the current-carrying cross-sectional area, while carbon doping into the $Mg(B_{1-x}C_x)_2$ grains also contributes to the decrease. However, $J_c(H)$ is much higher at high field in the doped samples. As pointed out in [3], an increase in H_{c2} leads to an increase of the pinning force at high magnetic fields, thus resulting in an enhancement of $J_c(H)$ even if the nature of the pinning is not changed (remains predominantly grain boundary pinning) or the number of pinning centers remains the same. Previously, we have shown in MO-doped films that the dominant pinning mechanism changes from grain boundary pinning to normal point pinning and back to grain boundary pinning when the carbon content increases [19]. These effects are believed to lead to high $J_c(H)$ in TMB-doped films as well. The results in figure 14 indicate that the effect on high-field

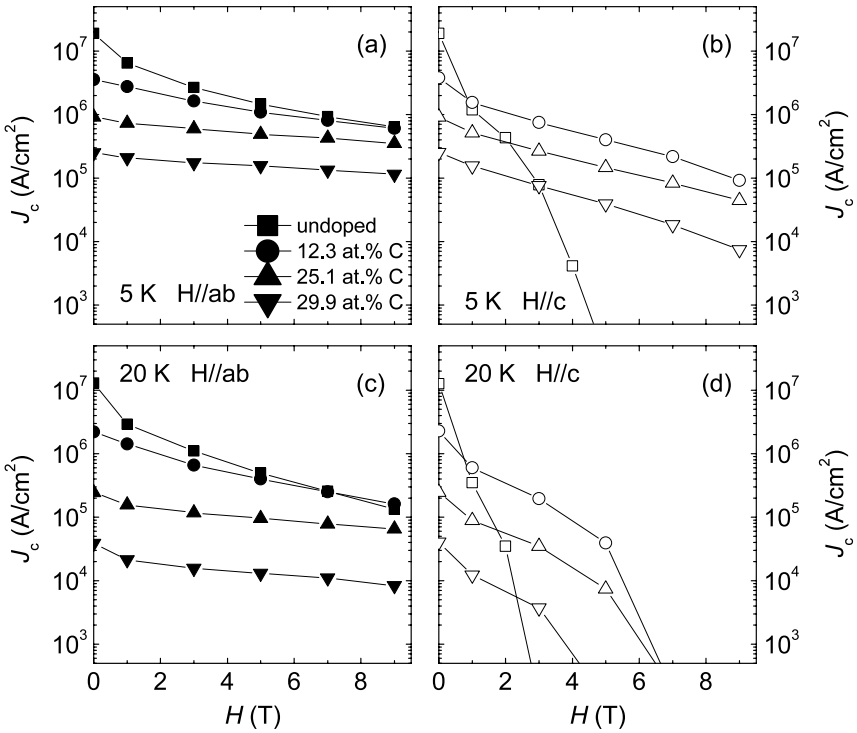

Figure 14. Magnetic field dependence of transport critical current density $J_c(H)$ for four different doping samples using a TMB source at 5 K for $H \parallel ab$ (a) and for $H \parallel c$ (b) and at 20 K for $H \parallel ab$ (c) and for $H \parallel c$ (d). The four samples have nominal carbon concentrations of 0, 12.3, 25.1 and 29.9 at.%, respectively. The lines are guides to the eye.

$J_c(H)$ is already evident at low doping and further doping to higher levels only results in lower overall J_c. At 5 K and $H = 9$ T, we have obtained $J_c \sim 6 \times 10^5$ A cm^{-2} for $H \parallel ab$ and $J_c \sim 1 \times 10^5$ A cm^{-2} for $H \parallel c$. Even at 20 K, $J_c > 10^5$ A cm^{-2} at 9 T for $H \parallel ab$ and $J_c > 10^4$ A cm^{-2} at 5 T for $H \parallel c$. These $J_c(H)$ values are very promising for applications of MgB_2 as high-field conductors.

4. Conclusion

In summary, we have studied the high-field properties of MgB_2 thin films carbon-doped by HPCVD using TMB as the carbon source and compared them with those of films doped with the MO source. For both cases, T_c decreases slowly and residual resistivity increases noticeably with carbon doping. The foreign phase MgB_2C_2 was found in the doped films by TEM, suggesting that only part of the carbon is doped into the MgB_2 lattice and the rest is in the carbon rich foreign phase in the grain boundaries. Unlike the case of bulk samples, both a and c lattice constants of carbon-doped MgB_2 films expand with carbon concentration. For carbon-doped films using both MO and TMB sources, carbon doping greatly enhances H_{c2}, attributed to the modification of interband and intraband scattering. In addition, films heavily doped by TMB show parallel H_{c2} over 70 T at low temperatures, close to the BCS paramagnetic limit, due to the unique microstructure consisting of MgB_2 layers a few nanometers thick spreading in the ab direction and separated by MgB_2C_2 layers. This multilayer structure explains the unusual behaviors including the high $H_{c2}^{\parallel}(T)$ slope and a downward curvature near T_c, the large H_{c2} anisotropy, and the 2D scaling behavior of angular dependence of $J_c(H)$. The high H_{c2} and high-field $J_c(H)$ values are very promising for high-field applications of MgB_2.

Acknowledgments

We acknowledge the support by the DOE under grant no. DE-FG02-08ER46531 (QL) and by ONR under grant no. N00014-07-1-0079 (XXX). Work at the University of Wisconsin was supported by funding from the DOE Office of Basic Energy Sciences under award number DE-FG02-06ER46327 (CBE).

References

[1] Nagamatsu J, Nakagawa N, Muranaka T, Zenitani Y and Akimitsu J 2001 *Nature* **410** 63
[2] Iwasa Y, Larbalestier D C, Okada M, Penco R, Sumption M D and Xi X X 2006 *IEEE Trans. Appl. Supercond.* **16** 1457
[3] Eisterer M 2007 *Supercond. Sci. Technol.* **20** R47
[4] Welp U *et al* 2003 *Physica* C **385** 154
[5] Zeng X H *et al* 2003 *Appl. Phys. Lett.* **82** 2097
[6] Xu S Y, Li Q, Wertz E, Hu Y F, Pogrebnyakov A V, Zeng X H, Xi X X and Redwing J M 2003 *Phys. Rev.* B **68** 224501
[7] Tarantini C *et al* 2006 *Phys. Rev.* B **73** 134518
[8] Cava R J, Zandbergen H W and Inumaru K 2003 *Physica* C **385** 8
[9] Dou S X, Braccini V, Soltanian S, Klie R, Zhu Y, Li S, Wang X L and Larbalestier D 2004 *J. Appl. Phys.* **96** 7549
[10] Bhatia M, Sumption M D, Collings E W and Dregia S 2005 *Appl. Phys. Lett.* **87** 042505
[11] Wilke R H T, Bud'ko S L, Canfield P C, Finnemore D K, Suplinskas R J and Hannahs S T 2004 *Phys. Rev. Lett.* **92** 217003

[12] Xi X X 2008 *Rep. Prog. Phys.* **71** 116501
[13] Angst M, Bud'ko S L, Wilke R H T and Canfield P C 2005 *Phys. Rev.* B **71** 144512
[14] Pogrebnyakov A V *et al* 2004 *Appl. Phys. Lett.* **85** 2017
[15] Pogrebnyakov A V *et al* 2005 *IEEE Trans. Appl. Supercond.* **15** 3321
[16] Braccini V *et al* 2005 *Phys. Rev.* B **71** 012504
[17] Ferdeghini C 2005 *IEEE Trans. Appl. Supercond.* **15** 3234
[18] Zhu Y, Larbalestier D C, Voyles P M, Pogrebnyakov A V, Xi X X and Redwing J M 2007 *Appl. Phys. Lett.* **91** 82513
[19] Chen J, Ferrando V, Orgiani P, Pogrebnyakov A V, Wilke R H T, Betts J B, Mielke C H, Redwing J M, Xi X X and Li Q 2006 *Phys. Rev.* B **74** 174511
[20] Zhuang C G, Meng S, Yang H, Jia Y, Wen H H, Xi X X, Feng Q R and Gan Z Z 2008 *Supercond. Sci. Technol.* **21** 82002
[21] Zhu Y, Hunte F, Zhuang C G, Feng Q R, Gan Z Z, Xi X X, Larbalestier D C and Voyles P M 2009 *Supercond. Sci. Technol.* **22** 125001
[22] Gurevich A 2003 *Phys. Rev.* B **67** 184515
Gurevich A 2007 *Physica* C **456** 160
[23] Zeng X H *et al* 2002 *Nature Mater.* **1** 35
[24] Xi X X *et al* 2007 *Physica* C **456** 22
[25] Lee S 2007 *Physica* C **456** 14
[26] Saengdeejing A, Saal J E, Wang Y and Liu Z K 2007 *Appl. Phys. Lett.* **90** 151920
[27] Rowell J M, Xu S Y, Zeng X H, Pogrebnyakov A V, Li Q, Xi X X, Redwing J M, Tian W and Pan X Q 2003 *Appl. Phys. Lett.* **83** 102
[28] Rowell J M 2003 *Supercond. Sci. Technol.* **16** R17
[29] Mickelson W, Cumings J, Han W Q and Zettl A 2002 *Phys. Rev.* B **65** 52505
[30] Lee S, Masui T, Yamamoto A, Uchiyama H and Tajima S 2003 *Physica* C **397** 7
[31] Bengtson A K, Bark C W, Giencke J, Dai W Q, Xi X X, Eom C B and Morgan D 2010 *J. Appl. Phys.* **107** 023902
[32] Gonnelli R S, Daghero D, Calzolari A, Ummarino G A, Dellarocca V, Stepanov V A, Kazakov S M, Zhigadlo N and Karpinski J 2005 *Phys. Rev.* B **71** 060503(R)
[33] Tsuda S, Yokoya T and Shin S 2007 *Physica* C **456** 126
[34] Szabo P, Samuely P, Pribulova Z, Angst M, Bud'ko S, Canfield P C and Marcus J 2007 *Phys. Rev.* B **75** 144507
[35] Putti M, Vaglio R and Rowell J M 2008 *Supercond. Sci. Technol.* **21** 043001
[36] Fletcher J D, Carrington A, Taylor O J, Kazakov S M and Karpinski J 2005 *Phys. Rev. Lett.* **95** 097005
[37] Sarma G 1963 *J. Phys. Chem. Solids* **24** 1029
[38] Gurevich A *et al* 2004 *Supercond. Sci. Technol.* **17** 278
[39] Kes P H, Aarts J, Vinokur V M and van der Beek C J 1990 *Phys. Rev. Lett.* **64** 1063
[40] Schmitt P, Kummeth P, Schultz L and Saemann-Ischenko G 1991 *Phys. Rev. Lett.* **67** 267
[41] Li Q, Kwon C, Xi X X, Bhattacharya S, Walkenhorst A, Venkatesan T, Hagen S J, Jiang W and Greene R L 1992 *Phys. Rev. Lett.* **69** 2713
[42] Labdi S, Kim S F, Li Z Z, Megtert S, Raffy H, Laborde O and Monceau P 1997 *Phys. Rev. Lett.* **79** 1381